Idealized Model for Equilibrium Boundary Layer over Land

ALAN K. BETTS

Atmospheric Research, Pittsford, Vermont

(Manuscript received 24 January 2000, in final form 10 July 2000)

ABSTRACT

An idealized equilibrium mixed layer (ML) model is used to explore the coupling between the surface, the ML, and the atmosphere above. It shows that ML depth increases as vegetative resistance to evaporation increases. The surface radiative forcing also increases ML depth; the ML radiative and evaporative cooling processes reduce ML depth. The model largely uncouples mean ML structure from the mean ML fluxes. The upper boundary condition controls ML potential temperature and mixing ratio but does not affect the fluxes; it is the surface radiative forcing and the radiative and evaporative cooling terms within the ML (together with the vegetative resistance R_v) that control the surface fluxes and evaporative fraction. Furthermore, for a given R_v, the radiative and evaporative cooling terms in the ML control the surface sensible heat flux, and the surface radiative forcing then controls the surface latent heat flux. The solutions show that, except for extreme high values of vegetative resistance and very dry air above the ML, this idealized equilibrium ML is capped by shallow cumulus clouds, as over the ocean. At the same time as R_v increases, the ML structure and depth shift from the oceanic limit toward a warmer, drier boundary layer. It is shown that surface evaporation controls equilibrium near-surface relative humidity and not vice versa. The equilibrium solutions also give insight into how the gradient of mean mixing ratio across the Mississippi River basin is linked to changes in surface pressure as well as vegetative resistance to evaporation. The equilibrium model is oversimplified, and the nonlinearities introduced by the diurnal cycle have not been addressed, but nonetheless the solutions are a plausible zero-order fit to daily mean model data for the Missouri and Arkansas–Red River basins and to summer composites from the First International Land-Surface Climatology Project Field Experiment.

1. Introduction

Understanding the surface climate equilibrium over land is important, if we are to assess the feedbacks associated with climate change. The land and ocean surfaces differ in two important ways. Water is not freely available for evaporation over land. In simple land surface models this is usually represented using an extra resistance to evaporation. In addition, the effective thermal capacity of the land surface is much smaller than the ocean mixed layer, so that there is a much larger diurnal cycle of temperature over land, driven by the diurnal cycle of the solar forcing at the surface. From a modeling perspective it is also significant that, unlike sea surface temperature (SST), maps of the land surface temperature (which is more heterogeneous than the ocean SST) are not routinely produced, and the availability of water for evaporation is not readily observed. As a result, in global and regional forecast models (in addition to climate models), all the fluxes and variables at the land surface are currently calculated. In contrast, in short- to medium-range forecast models, the ocean surface temperature is specified as an initial condition, and, in seasonal forecasting and climate modeling, the ocean boundary condition, like that over land, is also solved as a coupled problem. All forecast and climate models drift to their own ''model climate,'' and, if we can understand by using a simple model how the equilibrium climate at the land surface is determined (on timescales longer than the diurnal) by the coupling of the model physical parameterizations, then we can more easily correct the systematic biases of the model. Over the ocean, considerable progress has been made in understanding the surface and boundary layer (BL) equilibrium climate, especially in the Tropics, using simple bulk models such as those of Sarachik (1978), Betts and Ridgway (1988, 1989, 1992), Pierrehumbert (1995), and Clement and Seager (1999). The purpose of this paper is to address in part the analogous surface climate equilibrium over land for the midcontinental summer BL, which has received much less attention.

The simplification that will be made is to average over the diurnal cycle and to explore the interrelation of *diurnally averaged* state variables and fluxes, focusing primarily on the links to availability of water for evaporation. The analysis tool for understanding the daily average surface climate is a mixed boundary layer

Corresponding author address: Alan K. Betts, Atmospheric Research, 58 Hendee Lane, Pittsford, VT 05763.
E-mail: akbetts@aol.com

© 2000 American Meteorological Society

model. The mixed layer (ML) model has a long history, having been used for stratocumulus BLs by Lilly (1968) and for the dry BL by Betts (1973), Carson (1973), and Tennekes (1973). It will not, however, be used (as it is often is) to represent the growth of the daytime mixed layer driven by solar heating. Instead it will be used to represent a hypothetical daily average equilibrium ML, driven by the daily average surface net radiation budget and boundary conditions above the mixed layer. This approach needs further explanation. The diurnal cycle over land involves nonlinear processes at the surface, where the daytime BL is unstable and relatively well mixed and the nocturnal BL is strongly stable. Effective surface transfer coefficients are very different between day and night. It may seem surprising that an equilibrium model, which ignores this complexity in the diurnal cycle, could be of any value in understanding the daily average surface state. However, the motivation came from noticing the high level of structure in European Centre for Medium-Range Weather Forecasts (ECMWF) reanalysis daily average data, in relation to soil moisture, which invited a simple theoretical explanation. There is no doubt that more detailed studies with diurnally varying models will refine the details of the picture, but one intent of this paper is to show that the basic coupling of the surface thermodynamic variables and fluxes can be interpreted with a very simple equilibrium model. A second intent is to focus attention on the importance of explaining the mean diurnal state (and its longer timescale evolution), which is usually ignored by studies of the diurnal evolution of the BL (which are typically initialized with a morning BL state near sunrise).

I will first show the theoretical solutions of the equilibrium mixed layer model and then use two sets of data for illustration. One set is from the ECMWF reanalysis for the nine Julys from 1985 to 1993, averaged for the Red–Arkansas and Missouri River basins. This dataset was analyzed from an energy and hydrological perspective in Betts et al. (1998, 1999a). Although these data are purely model derived, they have the advantage of being extensive and complete, with a variable set coupled by the known model physical parameterizations (which may of course have formulation errors). A second, much smaller dataset (from Betts and Ball 1998) is the First International Land Surface Climatology Project Field Experiment (FIFE) data for the composite diurnal cycle for sets of days without rain in midsummer. This is a more limited dataset, covering only 53 days and representative of only a 15 km $\times$ 15 km area, but it has the advantage, of course, that it was derived from real observations. Last, the same data will be used to illustrate the relationship between the availability of soil water, diurnal averages, and the diurnal cycle of the surface lifting condensation level.

The observational studies of Betts and Ball (1995, 1998) and Betts et al. (1999b), as well as the studies with model data of Betts et al. (1998, 1999a), have shown the strong link between the availability of water for evaporation and the pressure height of the lifting condensation level or saturation level, or conversely the surface relative humidity, both in the daily average and in the daytime diurnal cycle. Heuristically, the drop of the mean saturation at the surface, between, for example, the saturation inside and the subsaturation outside a leaf surface, is clearly linked directly to the constraints on water evaporation. Indeed, this is one key difference between land and ocean. However, the low thermal capacity of the land surface means that the equilibrium temperature and humidity are tightly coupled. The idealized equilibrium solutions will show the dependence of all the thermodynamic variables (surface temperature, potential temperature, equivalent potential temperature, relative humidity, and saturation level) on the availability of water for evaporation and on thermodynamic parameters above the mixed layer. The analysis will illuminate how the mean surface energy partition (controlled by the availability of water for evaporation) controls the daily equilibrium temperature and humidity.

In a wider context, many papers have addressed the surface boundary condition over land and its effect on atmospheric circulations. Schär et al. (1999) discussed the soil moisture–precipitation feedback using a regional climate model over Europe and found their results were consistent with the earlier studies of Beljaars et al. (1996), Betts et al. (1996), and Eltahir (1998) in that high evaporation from wet soils led to a low Bowen ratio and low BL height. De Ridder (1997) used an ML model of the daytime BL to show that lower Bowen ratio led to higher equivalent potential temperature. In a later paper, De Ridder (1998) integrated a 1D model over a month of diurnal cycles to show the link between soil water surface evaporation and BL properties. However, the long-term equilibrium was controlled by relaxation terms. The model solutions shown in the next section directly address this long-term equilibrium by averaging over the diurnal cycle.

2. Idealized steady-state mixed layer model

The model is really a ''toy'' model for a hypothetical steady-state mixed layer over land. Bulk aerodynamic equations at the surface are coupled to an extension of the classic mixed layer model (Betts 1973; Carson 1973; Tennekes 1973). The surface forcing is the daily average net radiation, and the availability of water for evaporation at the surface is represented by a bulk vegetative resistance. Within the mixed layer, two diabatic processes are represented, radiative cooling and an evaporation of falling precipitation, which cools and moistens the mixed layer while conserving its equivalent potential temperature. A specified potential temperature gradient and saturation pressure difference [closely related to relative humidity (RH)] give the upper boundary condition for the mixed layer. Fluxes out of the mixed layer into ''clouds'' are represented by a vertical mass

flux, which is determined in equilibrium by imposing the constraint that the lifting condensation level (LCL), representing cloud base, equal the mixed layer depth. The model solutions are consistent with a positive cloud mass flux.

How does this toy equilibrium model relate to the mean diurnal cycle over land? During the daytime, the surface fluxes are large and the ML grows rapidly, briefly reaching a quasi equilibrium in the afternoon before collapsing at sunset. During the daytime, the BL growth is generally much larger than the mean subsidence, which is closely related in the mean to the radiative cooling as over the oceans (Betts and Ridgway 1988, 1989). Typically over land, a shallow cumulus layer forms at the top of the mixed layer, so that during most of the daytime hours, mixed layer depth and cloud-base height are tightly coupled. This convective flux out of the mixed layer into clouds is a more important constraint on daytime ML growth than is the mean subsidence. At night, the surface cools faster than the ML; a stable BL forms and grows during the night, influenced by radiative cooling, subsidence, and surface fluxes. The surface uncouples from the atmosphere and shallow clouds dissipate. What determines the long-term equilibrium, if conditions were the same day after day? In the thermal balance, there is a net upward surface sensible heat flux and a subsidence warming, which balances the net radiative cooling and, on some days, evaporative cooling of falling precipitation. In the moisture balance, a net upward latent heat flux balances a drying by subsidence, offset on some days again by the evaporation of falling precipitation. Diurnally integrated, these balances are similar over land as over the ocean, and we will use similar closures. The difference over land is that the surface fluxes are much larger in the daytime, when they are driven by the surface net radiation balance, and a mixed layer is generated with upward fluxes through cloud base; the fluxes are smaller at night. The steady-state solution, which averages over the stable and unstable BLs, is clearly not at all satisfactory in a quantitative sense, because, for example, representative surface transfer coefficients are hard to define, but the solutions are valuable qualitatively, because over the diurnal cycle the primary balances are between surface fluxes, radiation, and subsidence (and on some days the evaporation of precipitation).

a. Surface fluxes

The sensible (SH) and latent (LH) heat fluxes at the surface are driven by the net available energy Q^*, which will be specified. The balance can be written

$$Q^* = R_{\text{net}} - G = \text{SH} + \text{LH}, \tag{1}$$

where R_{net} and G are the diurnally averaged net radiation and ground heat fluxes (G will typically be small). The equations for the SH and LH fluxes can be written, following Monteith (1981), with θ_0 as a surface (aerodynamic) potential temperature (I shall ignore the difference between a surface sensible heat flux and a potential heat flux), as

$$\text{SH} = C_p F_{0\theta} = \rho C_p g_a(\theta_0 - \theta_M), \tag{2a}$$

$$\text{LH} = LF_{0q} = \rho L g_a(q_0 - q_M) = \rho L g_v[q_{s0}(T_0) - q_0]$$

$$= \rho L\left(\frac{g_v g_a}{g_a + g_v}\right)[q_{s0}(T_0) - q_M], \tag{2b}$$

where ρ and C_p are the density and heat capacity of air; L is the latent heat of evaporation; $F_{0\theta}$ and F_{0q} are the surface fluxes of potential temperature and moisture; θ_M and q_M are the potential temperature and specific humidity in the mixed layer; T_0, q_0, and q_{s0} are, respectively, the temperature, specific humidity, and saturation specific humidity at the surface; g_a is an aerodynamic conductance; and g_v is a vegetative conductance. As in the original Penman–Monteith solutions, given Q^* and the surface transfer coefficients, the surface temperature can be eliminated from (1) and (2), and the surface fluxes are then linked to the mixed layer solution for θ_M and q_M. The aerodynamic conductance will be nominally defined as

$$g_a = C_T V_s, \tag{3}$$

with a constant transfer coefficient $C_T = 10^{-2}$ (i.e., we neglect dependence on stability) and a constant mean wind speed of $V_s = 2.5$ m s^{-1} to give $g_a = 0.025$ m s^{-1}. The vegetative conductance is related to a vegetative resistance R_v by

$$g_v = 1/R_v. \tag{4}$$

This resistance is the parameter that controls the availability of water for evaporation at the surface and will be specified with the range from 60 to 900 s m^{-1}, representative of the range from well-watered grassland (Kim and Verma 1990) to the much higher resistance of the boreal forest under dry conditions with low RH (Betts et al. 1999b). The evaporative fraction defined as

$$\text{EF} = \text{LH}/(\text{LH} + \text{SH}) \tag{5}$$

will also be shown in some figures.

b. Mixed layer thermal and moisture balances

The thermal balance of the mixed layer can be written in pressure coordinates as

$$0 = \frac{P_H}{g}\frac{\partial \theta_M}{\partial t} = F_{0\theta} - F_{H\theta} + \left(\frac{\partial \theta_{\text{Rad}}}{\partial t} + \frac{\partial \theta_{\text{Evap}}}{\partial t}\right)(P_H/g). \tag{6}$$

The mixed layer depth is P_H (in pressure coordinates, defined to be positive), g is gravitational acceleration, $F_{H\theta}$ is defined in (8), $\partial\theta_{\text{Rad}}/\partial t$ is the mean mixed layer radiative cooling rate, and $\partial\theta_{\text{Evap}}/\partial t$ is a mean mixed layer cooling (both are defined to be negative) by the evaporation of falling precipitation (not to be confused with the surface evaporation). The roles of the two cool-

ing terms are similar in that both increase the equilibrium surface heat flux. The evaporation of falling precipitation, which could also be regarded as including cold convective outflows (both of which in reality are transient processes that disturb the ML structure), is included because it is clear that, on the basin scale, radiative cooling alone is not sufficient to explain the magnitude of the mean surface heat flux (see section 4 below).

The moisture balance can be written similarly as

$$0 = \frac{P_H}{g}\frac{\partial q_M}{\partial t} = F_{0q} - F_{Hq} - (C_p P_H/Lg)\frac{\partial \theta_{\text{Evap}}}{\partial t}, \quad (7)$$

where F_{Hq} is defined in (9).

c. ML-top fluxes

Fluxes out of the mixed layer at mixed layer top will be linked to jumps in θ and q and a combined subsidence and mass flux

$$F_{H\theta} = -\left(\frac{\Omega_T}{g}\right)\Delta\theta, \quad (8)$$

$$F_{Hq} = -\left(\frac{\Omega_T}{g}\right)\Delta q, \quad (9)$$

where

$$\Delta\theta = \theta_T - \theta_M \quad \text{and} \quad \Delta q = q_T - q_M. \quad (10)$$

The omega term, a cloud-base subsidence term, is the sum

$$\Omega_T = \Omega_R + \Omega_*, \quad (11)$$

where Ω_R is a radiative equilibrium subsidence (defined to be positive) at mixed layer top, and Ω_* is an additional mass flux (also defined to be positive) through cloud base, associated with a shallow cumulus field, typically the upward transport of air into clouds, that is moist but slightly cool (e.g., Betts 1975). Equations (8), (9), and (10) taken together assume that air that is removed from the mixed layer either by divergence or by rising to form clouds has mixed layer properties and is replaced by air with the properties θ_T and q_T.

d. ML-top boundary conditions

The boundary conditions at ML top are specified in terms of potential temperature and subsaturation. For potential temperature, we specify the profile

$$\theta_T = 303 + \Gamma(P_H - 60). \quad (12)$$

The stability Γ above the ML will be an external parameter that will be varied, and the reference ML depth of 60 hPa has been included, because this depth is close to the equilibrium for low resistance to evaporation (as over the ocean). Note that, in this simple model, any dependence of ''free-atmosphere'' potential temperature on surface pressure has been ignored, although a recent study by Molnar and Emanuel (1999) suggests that this effect is important over large surface height ranges.

Rather than specify q_T at ML top, the subsaturation (as the pressure height to the LCL of air) just above the mixed layer is given as a (variable) external parameter. A range will be considered,

$$\mathcal{P}_T = 60,\ 100,\ 140 \text{ hPa}, \quad (13)$$

characteristic of shallow cumulus over land. Mixing ratio above the mixed layer can be computed from surface pressure, ML depth, θ_T, and $\mathcal{P}_T$. The pressure height $\mathcal{P}_T$ to the LCL of air at pressure p_T with vapor pressure e has a very close relationship to $(1 - \text{RH}_T)$ through the formula (Betts 1997)

$$\mathcal{P}_T = p_T(1 - \text{RH}_T)/[A + (A - 1)\text{RH}_T], \quad (14)$$

where $\text{RH} = e/e_s$, e_s is the saturation vapor pressure, and $2A = [(\varepsilon L)/(C_p T)]$, where $\varepsilon = 0.622$ is the ratio of the gas constants for dry air and water vapor. The thermodynamic coefficient A increases slowly with decreasing temperature from 2.6 at 25°C to 3.4 at −40°C.

e. Closures

Two closures will be used. The first is the link between cloud-base virtual heat flux and surface virtual heat flux (Betts 1973; Tennekes 1973):

$$F_{H\theta_v} = -kF_{0\theta_v}, \quad \text{with } k = 0.2. \quad (15a)$$

If the closure were the slightly simpler one, with no virtual heat correction,

$$F_{H\theta} = -kF_{0\theta}, \quad \text{with } k = 0.2, \quad (15b)$$

then (6) reduces to just

$$1.2F_{0\theta} = -\left(\frac{\partial \theta_{\text{Rad}}}{\partial t} + \frac{\partial \theta_{\text{Evap}}}{\partial t}\right)(P_H/g). \quad (16)$$

Both the radiative and evaporative cooling will be treated as specified parameters, so these two and the ML depth can be regarded as determining the equilibrium surface sensible heat flux $\text{SH} = C_p F_{0\theta}$, as in Betts and Ridgway (1989). The surface energy balance equation [(1)] would then give LH.

However, using the virtual heat flux closure [(15a)] leads to a more complex formulation. From the definition of virtual temperature,

$$\theta_v = \theta(1 + 0.608q), \quad (17)$$

a virtual heat flux can be written in terms of the fluxes of sensible and latent heat, approximating $(0.608C_p\theta/L) \approx 0.073$, as

$$C_p F_{\theta_v} = C_p F_\theta + 0.073LF_q. \quad (18)$$

Adding 0.073 times (7) to (6) and rearranging gives the virtual heat flux balance of the ML, which together with closure (15b) gives

TABLE 1. Reference parameter set and ranges used.

Parameter	Reference	Range	Units
Aerodynamic conductance g_a	0.025	Fixed	m s^{-1}
Aerodynamic resistance l/g_a	40	Fixed	s m^{-1}
Vegetative resistance R_v	–	60–900	s m^{-1}
Entrainment parameter	0.2	0.2–0.3	–
Stability Γ	0.06	0.04–0.07	K (hPa)$^{-1}$
ML-top $\mathcal{P}_T$	100	60–140	hPa
Surface forcing Q^*	150	110–170	W m^{-2}
Radiative cooling rate	−3	−1 to −3	K day^{-1}
Evaporative cooling rate	0	0 to −3	K day^{-1}

$$(1+k)F_{0\theta_v} = F_{0\theta_v} - F_{H\theta_v} = -\left[\frac{\partial\theta_{\text{Rad}}}{\partial t} + (1-0.073)\frac{\partial\theta_{\text{Evap}}}{\partial t}\right](P_H/g). \quad (19)$$

Using (18) again for the surface fluxes, and substituting for the latent heat flux from (1), gives the following expression for surface sensible heat flux:

$$(1-0.073)\text{SH} = C_p(1-0.073)F_{0\theta} = -\left[\frac{\partial\theta_{\text{Rad}}}{\partial t} + (1-0.073)\frac{\partial\theta_{\text{Evap}}}{\partial t}\right] \times \{C_pP_H/[(1+k)g]\} - 0.073Q^*. \quad (20)$$

This equation appears to be complex, but without the virtual flux correction it reduces to (16). The key feature of (20) is that, given specified values for the surface radiative forcing Q^*, the net radiative cooling rate, and evaporative cooling rate, the surface SH flux is determined and is a linear function of ML depth P_H. From (1) the surface LH flux is also determined, as are the fluxes at ML top from (6) and (7), and they are all linear functions of P_H.

The second closure, which is perhaps deceptively simple, is to link ML depth to the LCL pressure height P_{LCL}, which is simply a function of θ_M and q_M that is,

$$P_H = P_{\text{LCL}}(\theta_M, q_M). \quad (21)$$

Conceptually, this closure can be considered as the one that primarily determines the cloud-base subsidence Ω_T, because increasing Ω_T reduces the mixed layer depth P_H and increases P_{LCL} through the drying and warming produced by the larger fluxes at mixed layer top. This closure will be justified later, when it will be shown that the equilibrium solutions require positive cloud-base mass flux, except in a ''dry'' limit of very large vegetative resistance and very dry air above the ML.

With this closure, all the fluxes at the surface and now at cloud base are all linear functions of cloud-base height. Note that RH_L of air at the base of the mixed layer is also directly related to P_{LCL} by a relationship similar to (14):

$$P_{\text{LCL}} = p_0(1-\text{RH}_L)/[A + (A-1)\text{RH}_L]. \quad (22)$$

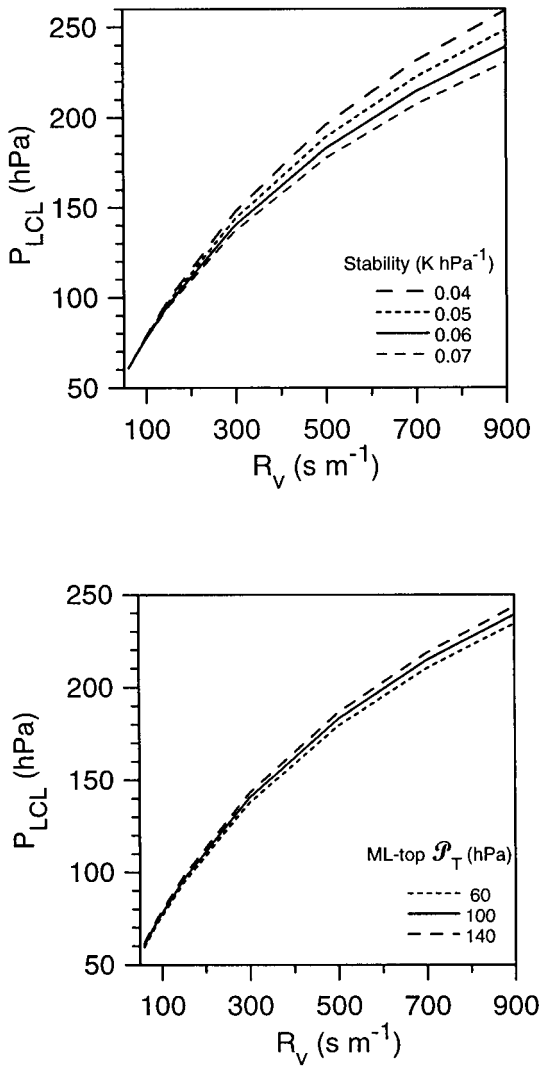

FIG. 1. Equilibrium ML depth as a function of R_v, for different values of the stability and $\mathcal{P}_T$ above the ML.

The system of Eqs. (1), (2), (6), (7), (8), (9), (10), (15a), (18), and (21) can be solved iteratively, given the surface transfer coefficients g_a and g_v, and the boundary conditions just above the mixed layer [(12) and (13)], as well as the equation of state and the Poisson equation. The solution converges over the whole range of R_v. Essentially, because P_{LCL} is a unique function of (θ_M, q_M), we look for the mixed layer pair (θ_M, q_M) that simultaneously satisfies the surface equations, the mixed layer budget equations, and the jump equations at cloud base. The equilibrium solutions couple surface fluxes and temperature and mixed layer properties to the free-atmosphere properties (θ_T, q_T) just above the ML.

3. Equilibrium model solutions

I will present most solutions with P_{LCL}, the pressure thickness of the ML, as the x axis because of the key

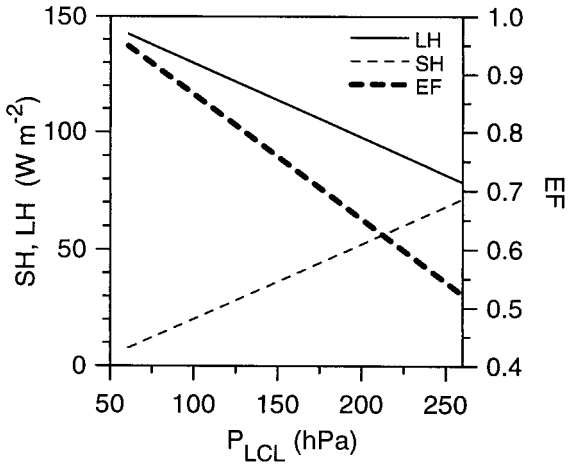

FIG. 2. SH, LH, and EF as a function of P_{LCL}.

role it plays in the SH budget closure [(20)]. This section discusses the relationship between vegetative resistance, equilibrium mixed layer depth, and the surface fluxes as a function of the external model parameters, which fall into two groups. The stability and RH_T (represented here by $\mathcal{P}_T$) above the ML affect the ML thermodynamic equilibrium but not the surface fluxes, for a given P_{LCL}. The surface radiative forcing Q^* and the radiative and evaporative cooling of the ML greatly affect the surface and ML-top fluxes but barely change the thermodynamic equilibrium, for a given P_{LCL}.

Table 1 shows the reference parameter set and the ranges used for sensitivity studies. In the figures showing model solutions, the reference parameter set is always the solid line. For the solutions in section 3, the surface pressure was fixed at 940 hPa, close to the mean pressure for the Arkansas–Red River basin, which is used for comparisons later in section 4.

a. Sensitivity of ML solutions to parameters above ML

First, Q^* and the radiative and evaporative cooling of the ML are fixed at their reference values, and the dependence on boundary conditions at ML top is explored. Figure 1a shows the monotonic increase of equilibrium ML depth P_{LCL} on the surface resistance to evaporation R_v and its weak dependence on stability above the ML (with $\mathcal{P}_T = 100$ hPa, corresponding to RH_T between 50% and 60%, depending on pressure). Figure 1b shows the even weaker dependence on $\mathcal{P}_T$, for the fixed reference stability above the ML of $\Gamma = 0.06$ K $(\mathrm{hPa})^{-1}$. This result suggests that the mean ML depth, which is well defined and observable during the daytime and is directly related to the near-surface RH_L through (14b), may be a useful surrogate for the surface resistance to evaporation, which is less easily observed. Consequently, P_{LCL} will be used as abscissa in many of the figures. Note that a high surface resistance to evaporation gives a deep mean ML, with equilibrium $P_{\mathrm{LCL}} \sim 250$ hPa. The dependence of P_{LCL} on the surface and radiative forcing will be shown later. Figure 2 shows the equilibrium surface fluxes and evaporative fraction [see (5)], which are linear functions of the ML depth P_{LCL} [see (20)]. These results are the equilibrium solutions to the ML model: LH decreases and SH increases with ML depth (here with the fixed sum of $Q^* = 150$ W m^{-2}), as R_v increases. Expressed in terms of P_{LCL}, *all the daily mean fluxes, including the ML-top fluxes, are independent* of both stability and $\mathcal{P}_T$ (or RH_T) above the ML. The linearity of EF with mean ML depth suggests that, given Q^* and radiative cooling rate, mean P_{LCL} may be a useful measure of mean evaporative fraction.

The ML parameters are dependent on the upper boundary condition, even though the fluxes are not. Figure 3 (left-hand panels) shows the slope of ML θ_M, q_M, and equivalent potential temperature θ_{EM} with P_{LCL} as the stability Γ above the ML increases (for $\mathcal{P}_T = 100$ hPa). As stability increases from 0.04 K $(\mathrm{hPa})^{-1}$ to 0.07 K $(\mathrm{hPa})^{-1}$, the slope of θ_M increases similarly, while q_M increases and its slope with P_{LCL} decreases. These solutions follow because the ML model tightly couples surface temperature and θ_M to θ_T, which has been defined by (12) and (21), and q_M to q_T. As a result, the trend of equilibrium θ_{EM} changes sharply from increasing slightly with ML depth at high stability to falling sharply with ML depth for the lowest stability shown, $\Gamma = 0.04$ K $(\mathrm{hPa})^{-1}$. This result is consistent with free-atmosphere θ_{ET} falling at a given pressure as Γ decreases, but $\mathcal{P}_T$ is fixed. The right-hand panels of Fig. 3 show the corresponding sensitivity to $\mathcal{P}_T$ (a measure of RH_T just above the ML) for $\Gamma = 0.06$ K $(\mathrm{hPa})^{-1}$. With drier air above, the ML gets drier and cooler because of increases in the jumps $\Delta\theta$ and Δq at ML top (see next section). The effect of drier, less-saturated air above the ML (larger $\mathcal{P}_T$), which has a lower θ_E, is a cooler, drier equilibrium ML, with a lower θ_{EM}.

b. Sensitivity of cloud-base jumps and mass flux to parameters above ML

For a given P_{LCL}, the fluxes at ML top or cloud base are independent of the stability and RH above the ML but the jumps in $\Delta\theta$ and Δq are not, because they depend on θ_T and q_T. What happens is that the jumps and the cloud-base subsidence term Ω_T adjust as shown in Fig. 4 to keep the cloud-base fluxes constant. The upper left panel of Fig. 4 shows the weak increase with stability of $\Delta\theta$ (heavy lines) and of $-\Delta q$ (lighter lines with q label). Correspondingly, Ω_T decreases with stability (lower left) to keep the cloud-base fluxes constant. On the right are the corresponding panels, which show a strong dependence on $\mathcal{P}_T$. With drier air above the ML (larger $\mathcal{P}_T$), Δq becomes more negative, Ω_T decreases, and $\Delta\theta$ increases. Note that the jump $(\theta_0 - \theta_M)$ across the surface superadiabatic layer, like the fluxes, is in-

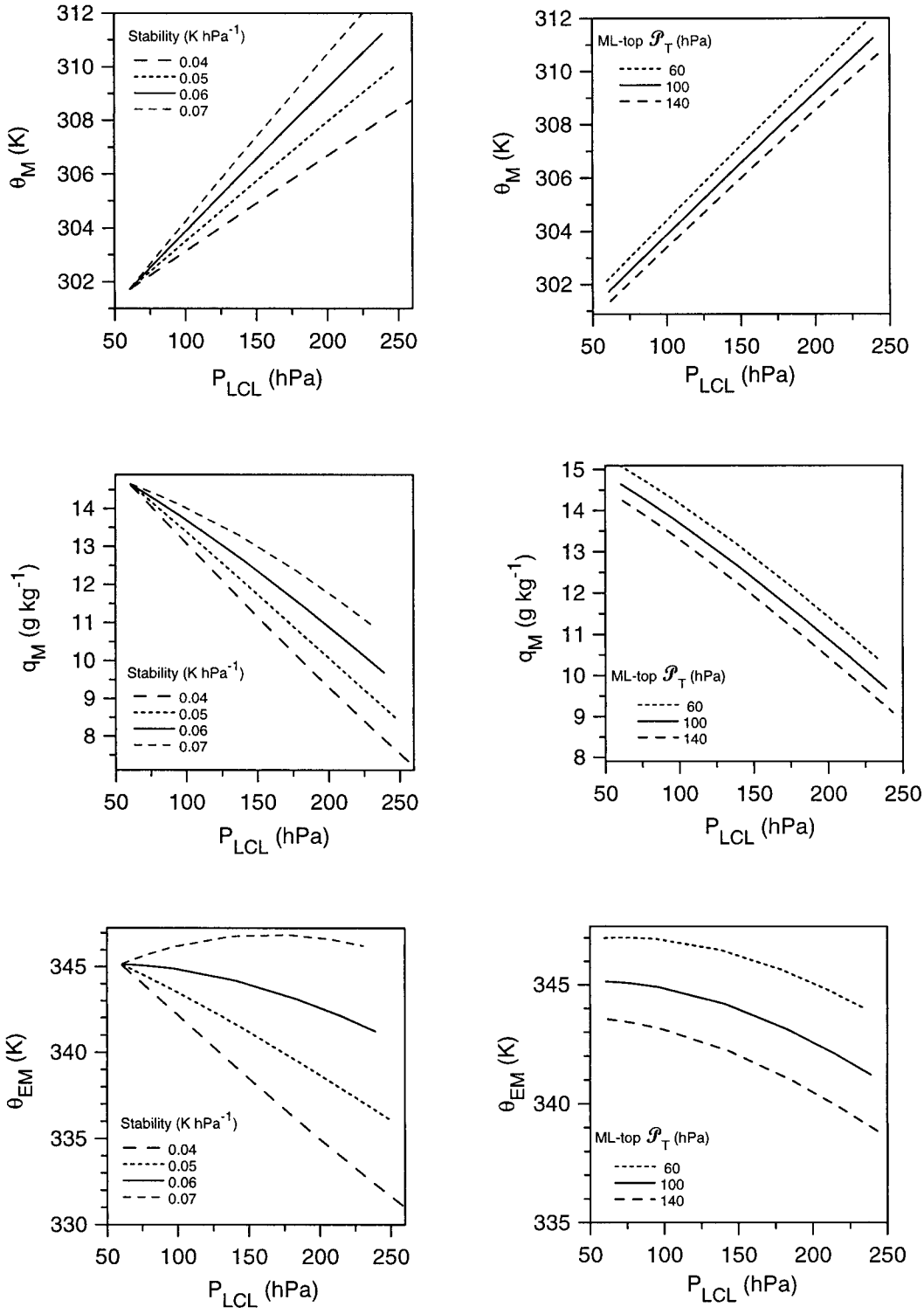

FIG. 3. Mixed layer equilibrium as a function of P_{LCL} for different values of the stability and $\mathcal{P}_T$ above the ML.

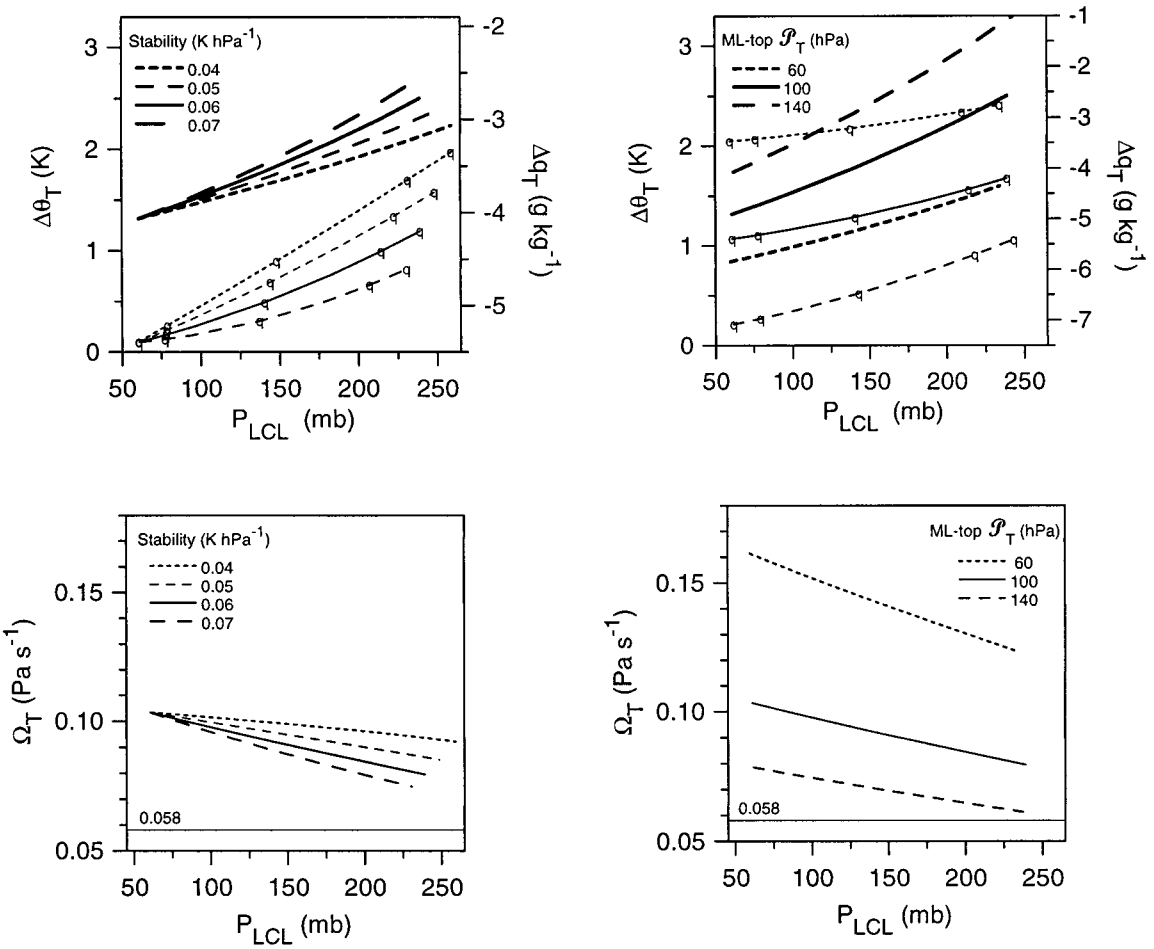

FIG. 4. Changes in ML-top jumps in θ and q, and subsidence parameter Ω_T for ranges of stability and $\mathcal{P}_T$ above the ML.

dependent of the parameters above the ML for a given P_{LCL}, so that the surface temperature is closely coupled to θ_M (for fixed Q^*).

A radiative equilibrium subsidence can be roughly estimated as

$$\Omega_R = -(\partial\theta_{\mathrm{Rad}}/\partial t)/\Gamma, \tag{23}$$

which, with $(\partial\theta_{\mathrm{Rad}}/\partial t) = -3\mathrm{K\ (day)^{-1}}$ and $\Gamma = 0.06$ K $(\mathrm{hPa})^{-1}$, gives $\Omega_R = 50$ hPa $(\mathrm{day})^{-1}$, or 0.058 Pa s^{-1}, which is indicated in the lower panels of Fig. 4. It can thus be concluded that the equilibrium ML solutions require a positive cloud-base mass flux, $\Omega_* > 0$, except for extreme limits of large R_v (giving large P_{LCL}) and large $\mathcal{P}_T$ (dry upper boundary condition). Therefore, except in this dry limit, the equilibrium ML over land, as over the ocean (Betts and Ridgway 1989), is capped by shallow cumulus clouds—a result that justifies the closure (21).

The mean entrainment parameter k was also varied, but the small sensitivity is not shown here because it is easily understandable. Increasing k from 0.2 to 0.3 increases the cloud-base jump of $\Delta\theta_v$ and cloud-base subsidence (to increase the θ_v flux), with a small increase of $\Delta\theta$, a small decrease in the size of Δq, and little change in the q flux at cloud base.

c. Sensitivity to Q* and ML radiative and evaporative cooling rates

The surface energy balance represented here by Q^*, and the radiative and evaporative cooling of the ML, affect the equilibrium depth and surface fluxes, but have less impact on the equilibrium ML parameters for a given depth. Figure 5 (left-hand panels) shows how, for a given vegetative resistance, ML depth increases with increasing surface forcing Q^*, decreases with increasing radiative cooling (because radiative cooling brings the ML closer to saturation), and decreases with increasing evaporative cooling of the ML (because this process cools and moistens toward saturation). In fact, the change in ML depth is almost identical, whether produced by radiative or evaporative cooling, because these changes have closely similar roles in (19). Figure 5 (right-hand panels) shows that, for a given ML depth, θ_M and q_M are little affected by changes in these energy forcing terms.

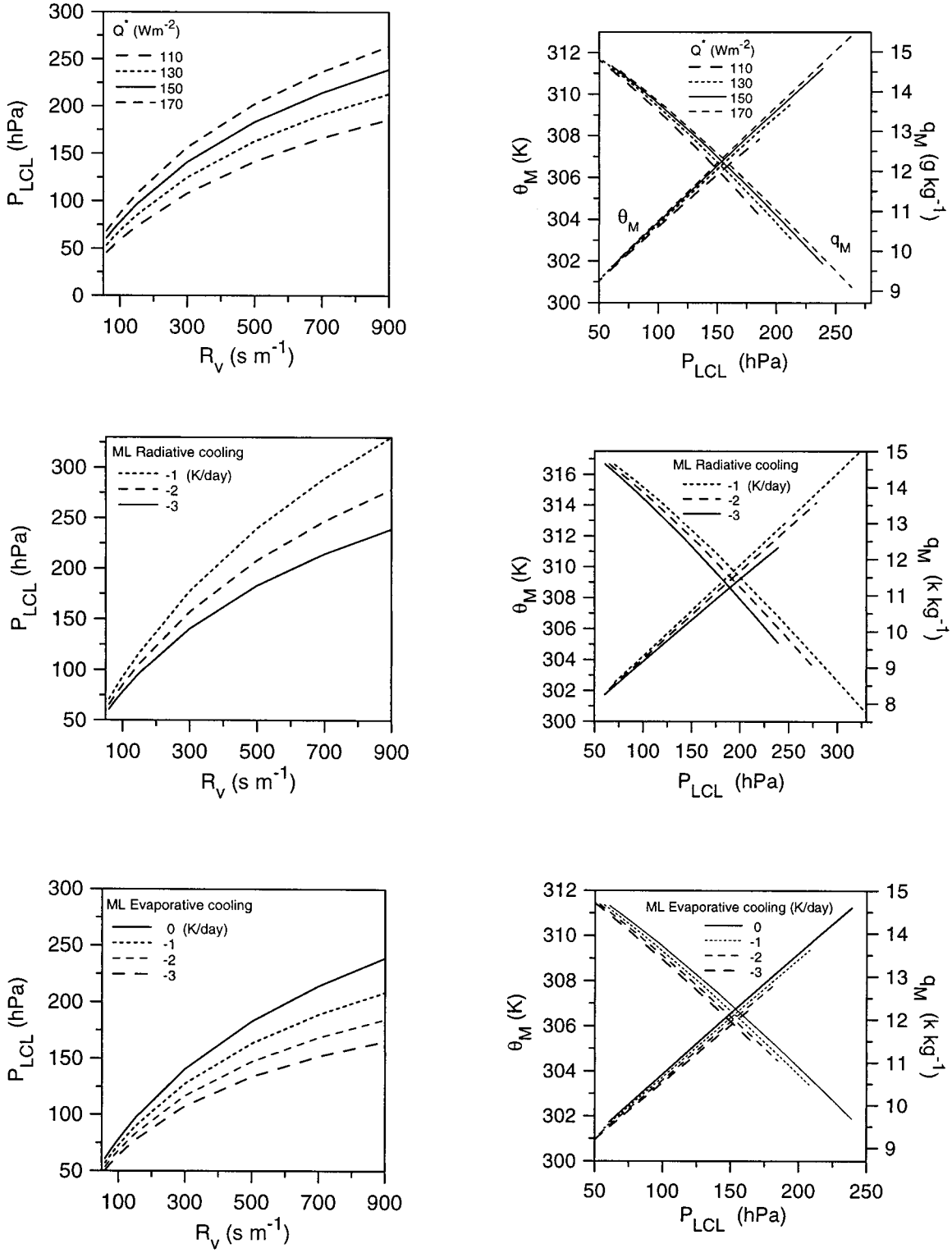

FIG. 5. (left) ML depth as a function of R_v for varying Q^*, ML radiative cooling, and ML evaporative cooling. (right) Similar for ML θ and q as a function of P_{LCL}.

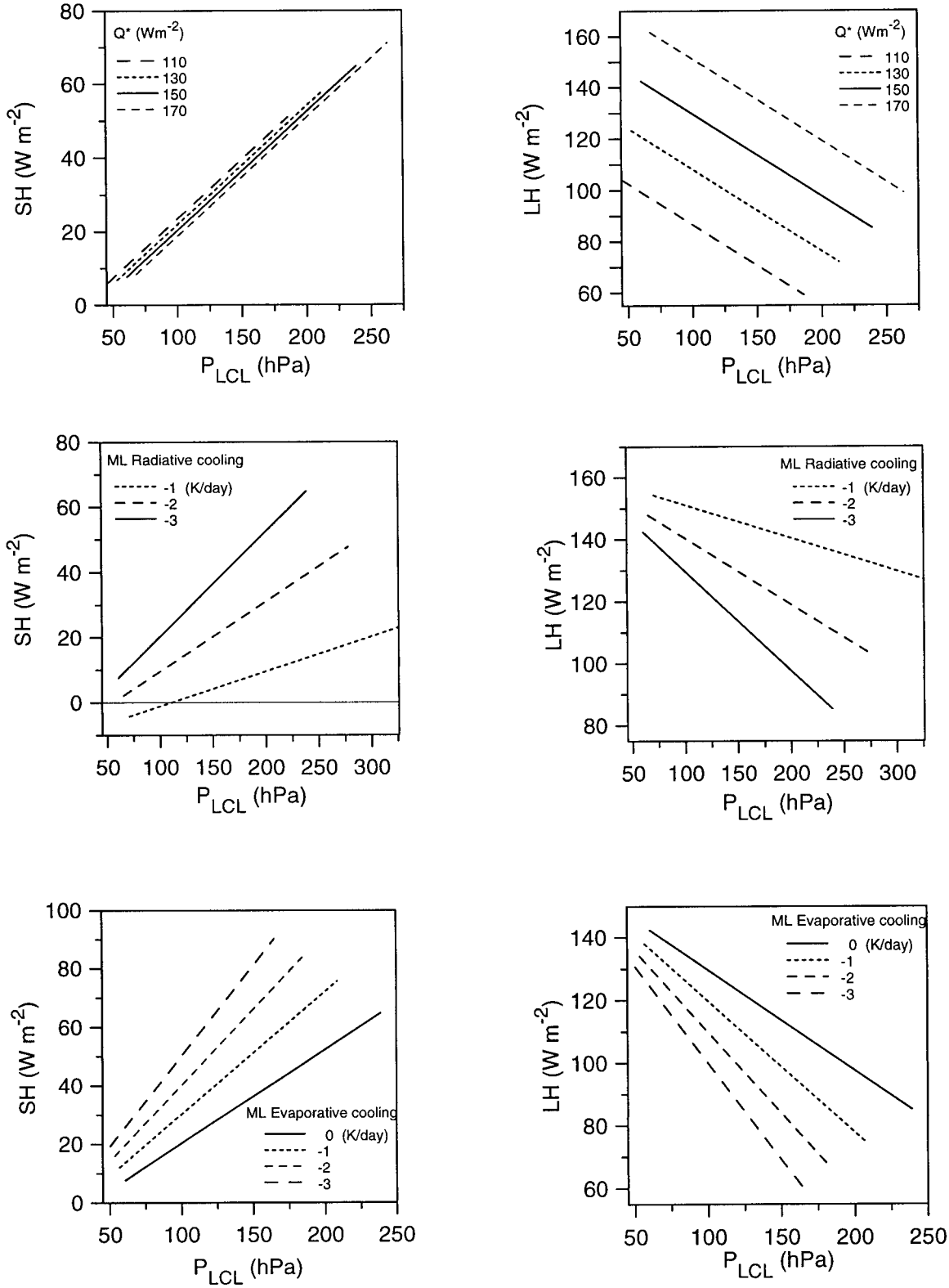

FIG. 6. Variation of (left) SH and (right) LH with ML depth, as a function of Q^*, ML radiative, and evaporative cooling (top to bottom).

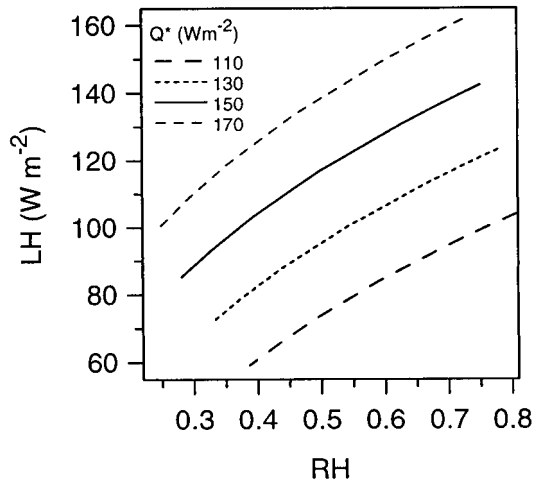

FIG. 7. Relationship between LH and near-surface RH as a function of Q^*.

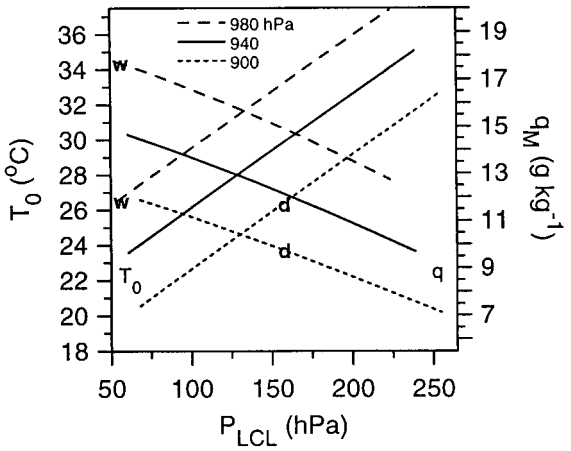

FIG. 8. Dependence of surface temperature and ML q on surface pressure and ML depth. Bold symbols **w** and **d** denote a low-elevation wet and an elevated dry surface, respectively.

Figure 6 shows the sensitivity of surface SH (left-hand panels) and LH (right-hand panels) to changes in the same flux forcing terms. Changes in Q^* have little effect on surface SH (because SH closely balances the internal ML cooling) but are projected almost entirely onto LH, so that EF increases with increasing Q^* (not shown). In contrast, radiative cooling (which cools θ_M at constant q_M) and evaporative cooling (which cools θ_M and increases q_M at constant θ_{EM}) have almost identical impacts on the surface energy budget: SH increases and LH decreases (as does EF) as radiative or evaporative cooling increases. This result is because the change in the surface SH flux is directly controlled by the cooling rate, through (20), and a cooling rate of 1 K day^{-1} corresponds to a flux divergence of about 12 W m^{-2} (100 hPa)$^{-1}$. The surface Q^* of 150 W m^{-2} then determines the surface LH. The result is that the solutions at the surface and for the ML are almost independent of whether the cooling is radiative or evaporative. However, the cloud-base fluxes do change: for the evaporative cooling case, the extra water evaporated is exported from the ML by larger cloud-base mass flux (which produces a small change in $\Delta\theta$). The important conclusion is that ML cooling determines equilibrium SH flux, and then ($Q^* - $ SH) determines the equilibrium LH flux.

d. Equilibrium relationship of surface evaporation and RH

Figure 7 plots the dependence of the surface LH flux on RH$_L$ at the base of the ML [related to $P_{\rm LCL}$ by (22)]. The LH flux increases with Q^* as expected, and the equilibrium near-surface RH$_L$ *decreases* as surface evaporation decreases. In the context of this equilibrium model, this result is obvious, but it is a sharp contrast to the nonequilibrium situation, in which evaporation increases if drier air blows over a wet surface. In the ML equilibrium over land, the resistance to evaporation (as well as Q^*) controls the LH flux, which, in turn, controls RH$_L$ and ML depth ($P_{\rm LCL}$). This result is also true of the typical diurnal cycle over land (see Fig. 13).

These solutions are different from the oceanic equilibrium discussed in Betts and Ridgway (1989), for which, in the absence of a corresponding additional resistance to evaporation, it is the radiative processes (together with the aerodynamic conductance) that control the surface energy balance, the near-surface RH, and the mean height of cloud base.

e. Dependence on surface pressure

Because the jumps in θ at the ML top (Fig. 4) and between surface and ML (not shown) are small, (12) largely determines the θ structure. If surface pressure is varied, the surface flux equilibrium is unaffected and θ_M is almost unchanged, because (12) is not a function of surface pressure. However, Fig. 8 shows that equilibrium q_M and the surface temperature both fall strongly with decreasing surface pressure for a given ML depth. In the next section, this model will be used to show that it is the difference in surface pressure, associated with the terrain elevation, that is linked to the difference in mixing ratio (and θ_E) between two datasets for the Missouri and Arkansas–Red River basins.

More generally, however, if we associate Fig. 8 with a midsummer east-to-west mean gradient across the Mississippi basin, vegetative resistance increases with the drier conditions in the west, caused by lower rainfall. The effects of falling surface pressure and higher R_v from east to west across the basin are additive for the fall of equilibrium q, but may partly cancel for the surface temperature change. The two states marked **w** and **d** for a wet surface at 980 hPa and an elevated dry surface at 900 hPa illustrate this point. They have the same surface equilibrium temperature of 26.5°C, but the

wet surface has an ML q of 17.6 g kg^{-1}, much greater than the dry elevated ML with a q of 9.8 g kg^{-1}. Mean cloud base increases from 60 hPa over the wet surface to 160 hPa over the elevated dry surface, and ML potential temperature and virtual potential temperature increase westward.

4. Comparison of equilibrium model with daily average data

Even though this idealized equilibrium model is not representative of the real world, it is of interest to see whether the solutions bear any relationship to daily averaged data. For this comparison surface or near-surface data are used.

a. Missouri and Arkansas–Red River basin datasets from ECMWF reanalysis

The first comparison is with model data from the first ECMWF reanalysis (ERA-15), and it is averaged over the Arkansas–Red and the Missouri basins, taken from Betts et al. (1999a). Figure 9 shows the daily averaged θ and q, calculated from the lowest model level (about 30 m above the surface) for 9 Julys from 1985 to 1993: on the left are the Arkansas–Red River basin averages, labeled 1, and on the right are those for the Missouri basin, labeled 2. The lines are the model solutions for the equilibrium ML, for a range of evaporation rates, calculated for the parameters given in Table 2. These parameters are the same for both basins, except for the mean basin surface pressure and Q*, which are the ERA-15 averages for the basins.

As in Fig. 5, the range of ML evaporative cooling rate has little effect here. The difference in q and θ_E between the basins, which is a consequence of the surface pressure difference, is largely captured by the model, even though closure (12) has no dependence on surface pressure. What is remarkable is that this idealized equilibrium model captures some of the day-to-day variability in the θ and q structure, despite having none of the dynamic or advective aspects of the processes over the Great Plains in summer.

Figure 10 shows the comparison of the model daily averaged surface SH and LH fluxes and the equilibrium model solutions. The scatter is large, but both basins show a similar result: the model, with a large ML cooling rate, captures some of the variability of the data. The best fit is for an evaporative cooling rate of order -2 K day^{-1} in addition to a radiative cooling rate of -3 K day^{-1}, which has not been varied in these figures. Because the model cannot distinguish at the surface between these cooling processes (see section 3c), all that can be concluded is that the ERA-15 daily averaged fluxes are consistent with the equilibrium model for a large ML cooling rate of -5 K day^{-1}. This result suggests that, on the basin scale in summer, the evaporation of falling precipitation is playing a significant role in the BL energy balance on most days (at least in ERA-15).

Figure 11 shows the correlations that prompted this equilibrium model. The upper panel is the tight correlation between the volumetric soil water in the first model soil layer (0–7 cm) with P_{LCL}. Soil water is an important control on vegetative resistance to transpiration in the model. Both basins are shown, and they cannot be distinguished. Betts et al. (1999a) found that this relationship does not depend on surface pressure or temperature across all Mississippi basins. The lower panel shows the correlation between the lowest model temperature (at roughly 30 m above the surface) and P_{LCL}: there is a similar tight correlation with first model soil layer temperature. The lines are the corresponding equilibrium model solutions for T_M, calculated from θ_M, and the surface pressure. The agreement is good, showing that the daily averaged temperatures are consistent with the equilibrium model.

b. FIFE summer composites

The second comparison is with daily averaged summer FIFE composites taken from Betts and Ball (1998). The data are daily mean near-surface data, consisting of six averages of between 7 and 10 days from two summers, composited according to ranges of soil water. (The diurnal cycle for these same composites are shown later in section 5 and in Fig. 13b.) Figure 12 shows the fit of the equilibrium model to these data for the parameters in Table 2. The mean surface pressure, Q*, and surface wind for the FIFE data have been used. The stability Γ and cloud-top $\mathcal{P}_T$ have been chosen to give the best fit to the data, and the values (in Table 2) are consistent with the FIFE sonde data (Betts and Ball 1994), although sonde data are not available for all the days in the composite. The observed trend from warm, dry near-surface air to cooler, moister air coupled to increasing P_{LCL} (in the upper panel) corresponds to increasing soil water. In the model, the dependence is on R_v. The second panel compares model and observed θ_E and surface temperature, T_o. In this case, the data are the observed radiometric skin temperatures. Although the data are noisy, the agreement is reasonable. The lower panel compares equilibrium model surface SH and LH fluxes with the observed daily averages. The fit is good for a total ML cooling of -4 K day^{-1}, which was modeled as a radiative cooling of -3 K day^{-1} and a small evaporative cooling of -1 K day^{-1} (which is consistent with these being days without significant surface precipitation).

5. Comment on the relationship between soil water, diurnal averages, and the diurnal cycle of P_{LCL}

These same data from ERA-15 and FIFE give some insight into the relationship of shifts in the daily mean

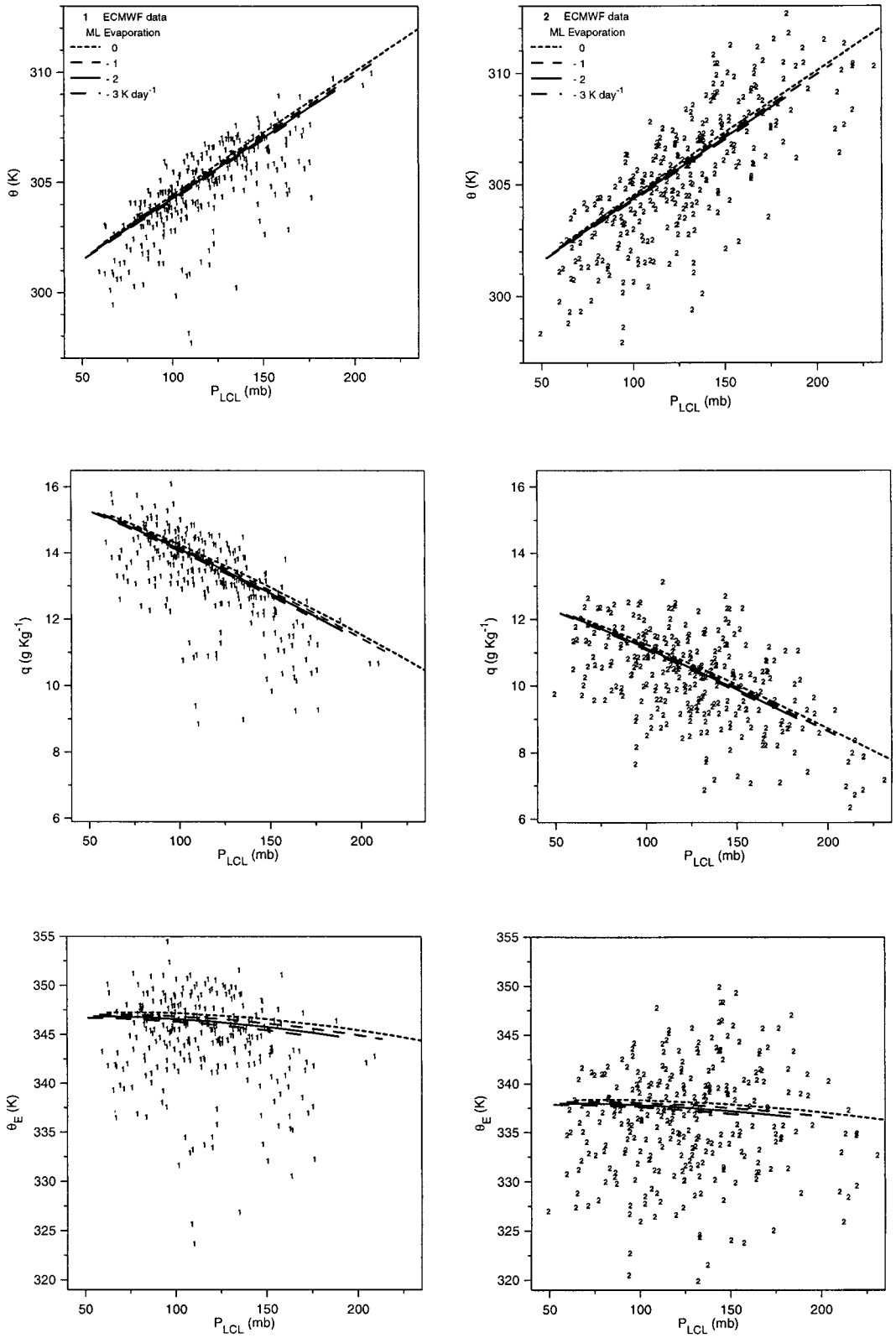

FIG. 9. Daily average potential temperature, specific humidity, and equivalent potential temperature against P_{LCL} for the month of Jul 1985–93 for the Arkansas–Red basin (marked as 1) and the Missouri basin (marked as 2) and equilibrium mixed layer model fits for a range of ML evaporation.

TABLE 2. Parameter sets for data comparison.

Parameter	Arkansas–Red	Missouri	FIFE	Units
Aerodynamic conductance g_a	0.025	0.025	0.049	m s^{-1}
Aerodynamic resistance, $1/g_a$	40	40	20.4	s m^{-1}
Vegetative resistance R_v	60–900	60–900	60–900	s m^{-1}
Entrainment parameter	0.2	0.2	0.2	–
Stability Γ	0.06	0.06	0.05	K (hPa)$^{-1}$
ML-top $\mathcal{P}_T$	60	60	80	hPa
Surface pressure	941	896	970	hPa
Surface forcing Q^*	158	141	167	W m^{-2}
Radiative cooling rate	−3	−3	−3	K day^{-1}
Evaporative cooling rate	0 to −3	0 to −3	−1	K day^{-1}

to shifts in the diurnal pattern. The data have been binned by soil water, which is a control on vegetative resistance in summer in both the ERA model and the FIFE data. Figure 13a shows the mean diurnal cycle of P_{LCL}, corresponding to the data in Fig. 11a for the Missouri river basin for the month of July 1985–93, binned by volumetric soil water SW1 in the model 0–7-cm soil layer (using 0.02 intervals). The entire diurnal cycle is shifted upward with decreasing soil water. Although the daytime amplitude of this shift is a little larger than the

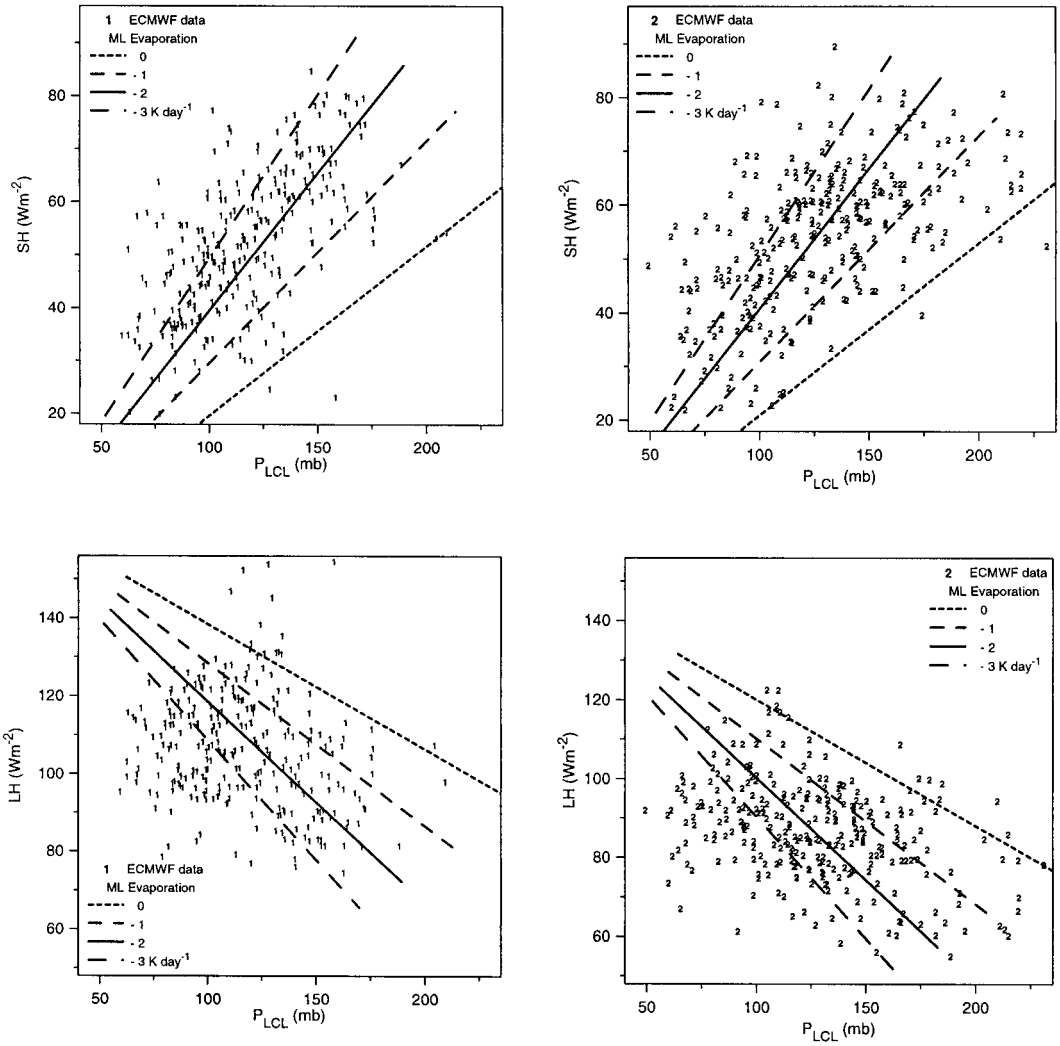

FIG. 10. Daily average SH and LH against P_{LCL} for the month of Jul 1985–93 for the Arkansas–Red basin (shown by 1) and the Missouri basin (shown by 2) and equilibrium mixed layer model fits for a range of BL evaporation.

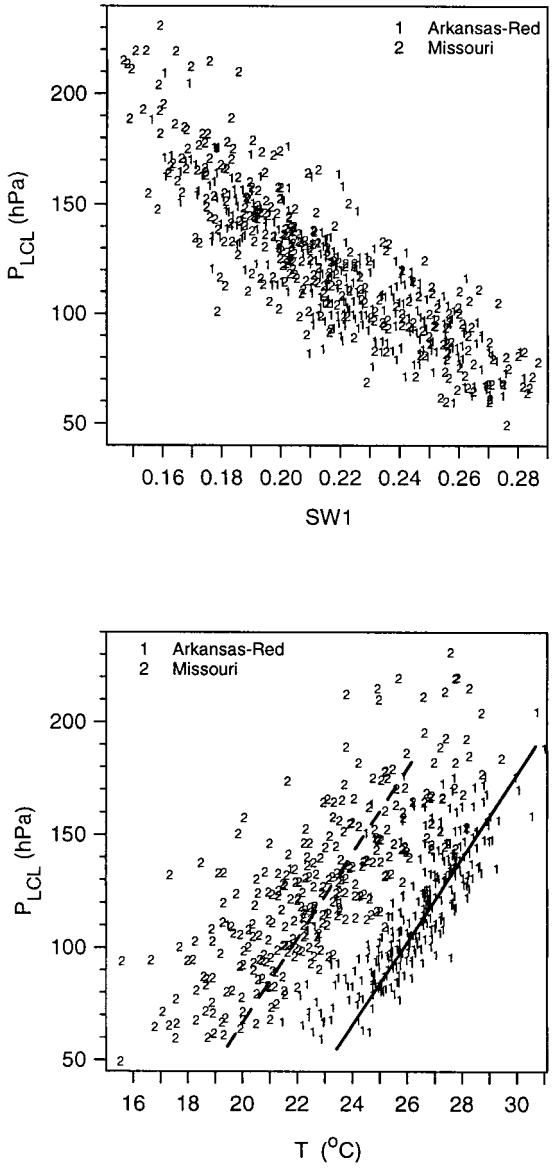

FIG. 11. (top) Dependence of P_{LCL} on soil water SW1 for first model ground layer (0–7 cm); (bottom) relation between P_{LCL} and lowest model-level atmospheric temperature. Lines are equilibrium model solutions.

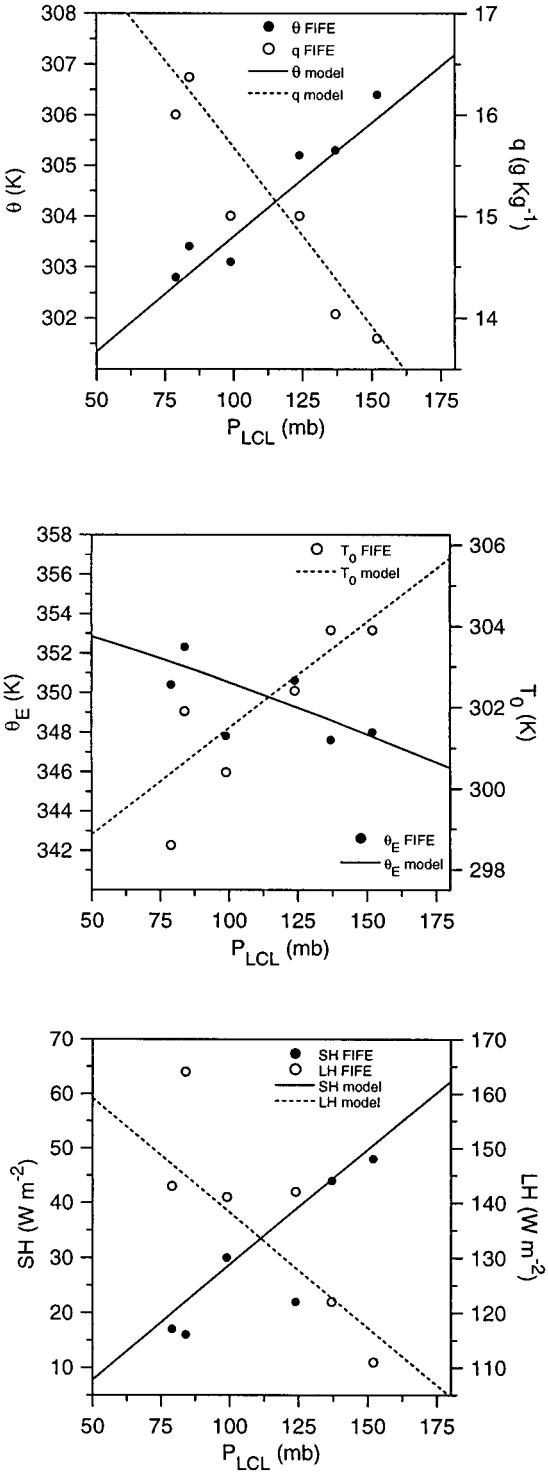

FIG. 12. Comparison of equilibrium solutions and FIFE summer composites. (top) Potential temperature and mixing ratio. (middle) Equivalent potential temperature and surface temperature. (bottom) Sensible and latent heat fluxes.

nighttime amplitude, it is clear that the daily mean shift with soil water is representative of both daytime and nighttime processes. Figure 13b shows the corresponding figure for the midsummer FIFE averages (from section 4b) binned by volumetric soil water (in the 0–10-cm layer), as discussed in more detail in Betts and Ball (1998). The sample size is smaller (only 7–10 days in each average), and, as in Fig. 12, the progression is not entirely uniform, but the general pattern is the same as that for ERA-15. The observations show a slightly smaller range for a similar range of soil water, and a sharper fall of P_{LCL} in the evening (local noon is around 1800 UTC), when compared with the ERA-15 com-

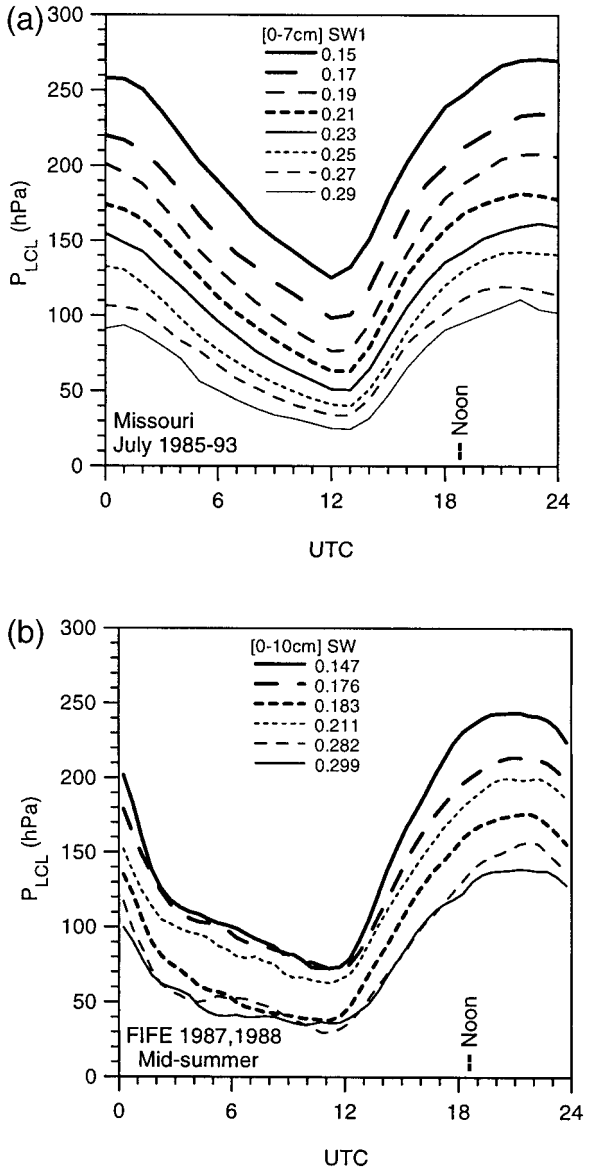

FIG. 13. Mean diurnal cycle, stratified by soil moisture, for (a) Missouri basin for Jul 1985–93 and (b) FIFE 1987 and 1988 mid-summer composites. Local noon (near 1830 UTC) is marked.

posites. Figure 13 shows that soil water decreases, which are linked to increases in vegetative resistance, produce an upward mean shift of saturation pressure height P_{LCL}, as well as some amplification of the diurnal cycle of P_{LCL}.

6. Conclusions

This equilibrium ML model, although highly simplified, suggests several important conclusions about the coupling between the surface, the ML, and the atmosphere above on timescales longer than the diurnal. First, it shows that the mean ML depth increases as vegetative resistance to evaporation increases. In addition, the surface radiative forcing also increases ML depth, but the ML radiative and evaporative cooling processes reduce ML depth. Second, the model largely uncouples mixed layer parameters, as defined by ML θ and q, from the ML fluxes. The boundary conditions above the ML control θ and q but do not affect the fluxes; it is the surface forcing Q^* and the radiative and evaporative cooling terms within the ML (together with the vegetative resistance) that control the mean surface fluxes and evaporative fraction. Furthermore, for a given R_v, it is the radiative and evaporative cooling terms that control the surface SH flux; the surface forcing Q^* then controls the LH flux.

The solutions show that, except for extreme values of vegetative resistance and very dry air above the ML, the equilibrium ML is capped by shallow cumulus clouds, as over the ocean. At the same time, as R_v increases, the ML structure and depth shift from the oceanic limit toward a warmer, drier boundary layer. The model shows that evaporation controls equilibrium near-surface RH and not vice versa. The equilibrium solutions also give insight into how the gradient of mean mixing ratio across the Mississippi basin is linked to changes in surface pressure as well as vegetative resistance to evaporation.

An equilibrium model is over simplified, and the non linearities introduced by the diurnal cycle have not been addressed, but nonetheless the solutions are a plausible zero-order fit to daily mean model data for the Missouri and Arkansas–Red River basin averages, shown in Figs. 9 and 11, and summer composites from the FIFE experiment, shown in Fig. 12. The river basin comparisons suggest that evaporation of falling precipitation plays a significant role in determining the mean surface fluxes on this scale. These same data give some insight into the relationship of shifts in the daily mean to shifts in the diurnal pattern. Figure 13 shows that decreases in soil water, which are linked to increases in vegetative resistance, produce an upward mean shift of saturation pressure height P_{LCL}, as well as some amplification of the diurnal cycle of P_{LCL}.

The upper boundary closure on potential temperature [12] is an over simplification, although it is also broadly consistent with the Missouri and Arkansas–Red River basin averages. A recent radiative convective equilibrium study of temperature profiles at different heights by Molnar and Emanuel (1999) suggests that potential temperature profiles may be coupled with surface height above sea level, not just with pressure height above the surface, as in (12). In addition, by using the closure, represented by (13), the ML and shallow cumulus layers have been uncoupled, and clearly their coupling deserves further study. However, this simple model is likely to be useful in separating the effect of upper boundary conditions and internal processes on the mean surface equilibrium over land, and in understanding feedbacks at the land surface in coupled models.

Acknowledgments. I acknowledge support from the National Science Foundation under Grant ATM-9988618, from NOAA under Grant NA76-GP0255, and from NASA under Grant NAG5-8364. I am grateful to the reviewers for their helpful comments.

REFERENCES

Beljaars, A. C. M., P. Viterbo, M. J. Miller, and A. K. Betts, 1996: The anomalous rainfall over the United States during July 1993: Sensitivity to land surface parameterization and soil moisture anomalies. *Mon. Wea. Rev.*, **124,** 362–383.

Betts, A. K., 1973: Non-precipitating convection and its parameterization. *Quart. J. Roy. Meteor. Soc.*, **99,** 178–196.

——, 1975: Parametric interpretation of trade-wind cumulus budget studies. *J. Atmos. Sci.*, **32,** 1934–1945.

——, 1997: The parameterization of deep convection. *The Physics and Parameterization of Moist Atmospheric Convection*, R. K. Smith, Ed., NATO ASI Series C, Vol. 505, Kluwer Academic, 255–279.

——, and W. Ridgway, 1988: Coupling of the radiative, convective, and surface fluxes over the equatorial Pacific. *J. Atmos. Sci.*, **45,** 522–536.

——, and ——, 1989: Climatic equilibrium of the atmospheric convective boundary layer over a tropical ocean. *J. Atmos. Sci.*, **46,** 2621–2641.

——, and ——, 1992: Tropical boundary layer equilibrium in the last ice age. *J. Geophys. Res.*, **97,** 2529–2534.

——, and J. H. Ball, 1994: Budget analysis of FIFE 1987 sonde data. *J. Geophys. Res.*, **99,** 3655–3666.

——, and ——, 1995: The FIFE surface diurnal cycle climate. *J. Geophys. Res.*, **100,** 25 679–25 693.

——, and ——, 1998: FIFE surface climate and site-average dataset: 1987–1989. *J. Atmos. Sci.*, **55,** 1091–1108.

——, ——, A. C. M. Beljaars, M. J. Miller, and P. Viterbo, 1996: The land-surface–atmosphere interaction: A review based on observational and global modeling perspectives. *J. Geophys. Res.*, **101,** 7209–7225.

——, P. Viterbo, and E. Wood, 1998: Surface energy and water balance for the Arkansas–Red River basin from the ECMWF reanalysis. *J. Climate,* **11,** 2881–2897.

——, J. H. Ball, and P. Viterbo, 1999a: Basin-scale surface water and energy budgets for the Mississippi from the ECMWF reanalysis. *J. Geophys. Res.*, **104,** 19 293–19 306.

——, M. L. Goulden, and S. C. Wofsy, 1999b: Controls on evaporation in a boreal spruce forest. *J. Climate,* **12,** 1601–1618.

Carson, D. J., 1973: The development of a dry inversion-capped convectively unstable boundary layer. *Quart. J. Roy. Meteor. Soc.*, **99,** 450–467.

Clement, A., and R. Seager, 1999: Climate and the tropical oceans. *J. Climate*, **12,** 3383–3401.

De Ridder, K., 1997: Land surface processes and the potential for convective precipitation. *J. Geophys. Res.*, **102,** 30 085–30 090.

——, 1998: The impact of vegetation cover on Sahelian drought persistence. *Bound.-Layer Meteor.*, **88,** 307–321.

Eltahir, E. A. B., 1998: A soil moisture rainfall feedback mechanism. 1: Theory and observations. *Water Resour. Res.*, **34,** 765–776.

Kim, J., and S. B. Verma, 1990: Components of the surface energy balance in a temperate grassland ecosystem. *Bound.-Layer Meteor.*, **51,** 401–417.

Lilly, D. K., 1968: Models of cloud-topped mixed layers under a strong inversion. *Quart. J. Roy. Meteor. Soc.*, **94,** 292–309.

Molnar, P., and K. A. Emanuel, 1999: Temperature profiles in radiative–convective equilibrium above surfaces at different heights. *J. Geophys. Res.*, **104,** 24 265–24 271.

Monteith, J. L., 1981: Evaporation and surface temperature. *Quart. J. Roy. Meteor. Soc.*, **107,** 1–21.

Pierrehumbert, R. T., 1995: Thermostats, radiator fins, and the runaway greenhouse. *J. Atmos. Sci.*, **52,** 1784–1806.

Sarachik, E. S., 1978: Tropical sea surface temperature: An interactive one-dimensional atmosphere–ocean model. *Dyn. Atmos. Oceans*, **2,** 450–469.

Schär, C., D. Lüthi, U. Beyerle, and E. Heise, 1999: The soil–precipitation feedback: A process study with a regional climate model. *J. Climate,* **12,** 722–741.

Tennekes, H. A., 1973: Model for the dynamics of the inversion above a convective boundary layer. *J. Atmos. Sci.,* **30,** 558–567.